PAPER VIII

Wall effects on space averaged two-fluid model equations for simulations of gas–solid flows in risers

Chemical Engineering Science 89 (2013) 206–215.

Chemical Engineering Science 89 (2013) 206–215

Contents lists available at SciVerse ScienceDirect

Chemical Engineering Science

journal homepage: www.elsevier.com/locate/ces

Wall effects on space averaged two-fluid model equations for simulations of gas–solid flows in risers

Srujal Shah [a,*], Jouni Ritvanen [a], Timo Hyppänen [a], Sirpa Kallio [b]

[a] LUT Energy, Faculty of Technology, Lappeenranta University of Technology, P.O. Box 20, FI-53851 Lappeenranta, Finland
[b] VTT Technical Research Centre of Finland, P.O. Box 1000, FI-02044 VTT, Finland

HIGHLIGHTS

- Two-fluid model was used for numerical simulation of gas–solid flow in a riser with Geldart group B particles.
- Space averaging applied over the gas–solid drag and the convective term to analyze the subgrid-scale modeling.
- Wall effects were studied for subgrid-scale models.
- Subgrid-scale models showed dependence on distance from the wall, averaging size and solid volume fraction.
- Results obtained for Geldart group B particles clearly differ from those presented in the literature for Geldart group A particles.

ARTICLE INFO

Article history:
Received 4 June 2012
Received in revised form
15 September 2012
Accepted 16 November 2012
Available online 5 December 2012

Keywords:
Circulating fluidized bed
Computational fluid dynamics
Two-fluid model
Space averaging
Subgrid-scale models
Wall effects

ABSTRACT

For the study of gas–solid flows in a circulating fluidized bed (CFB) riser, the model based on the Eulerian description of phases is widely used. Such a description requires the usage of a fine mesh and a short time step in the numerical simulations. Due to the constraint of long calculation times with fine meshes, it becomes practical to simulate the gas–solid flow in a CFB riser with coarse meshes. This work is the continuation of formulating the subgrid-scale models for the space averaged two-fluid model equations which can be used in coarse mesh simulations of gas–solid flows in risers. In this study, the vertical component of the drag force and the convective term are analyzed and their dependence on the averaging size and solid volume fraction with the distance from the wall is presented.

1. Introduction

Multiphase flows in industrial units such as circulating fluidized beds are heterogeneous and exhibit large fluctuations over spatiotemporal scales. The modeling of gas–solid two-phase flows in a CFB riser is mainly done with the use of a two-fluid model (Anderson and Jackson, 1967; Gidaspow, 1994; Lun et al., 1984). In the two-fluid model formulation, both phases are treated as interpenetrating continua. The continuity and momentum equations are solved for both phases. The closure models for the solid phase momentum equation based on the kinetic theory of granular flow can well predict the core-annulus flow regime (Benyahia et al., 2007).

Computational fluid dynamics (CFD) simulation of gas–solid flows using a two-fluid model usually requires a very fine mesh to capture the mesoscale structures. This restricts the simulation of large scale fluidized bed units because of infeasible calculation time. For practical calculation purposes, the gas–solid flows in risers are usually simulated with coarse meshes, and as a result, the information about the mesoscale structures in the flow field is lost. This lost information about the mesoscale structures must be retrieved in the form of appropriate closure models when performing coarse mesh size simulations. Many attempts have been made by various research groups for the formulation of closures which can be used in coarse mesh simulations of gas–solid flows in risers (Agrawal et al., 2001; De Wilde, 2005; Igci et al., 2008; Wang and Li, 2007; Yang et al., 2004; Zhang and VanderHeyden, 2002).

When Reynolds averaging is applied to the Navier–Stokes equations as in the single phase flow, there is a need to model the Reynolds stresses which arise from the velocity fluctuations.

* Corresponding author. Tel.: +358 40 173 5672.
E-mail address: srujal.shah@lut.fi (S. Shah).

0009-2509/$ - see front matter © 2012 Elsevier Ltd. All rights reserved.
http://dx.doi.org/10.1016/j.ces.2012.11.020

Similarly, for two-phase gas–solid flows, the macroscopic averaging approach, also known as filtering approach, is applied over the equations. Different macroscopic averaging approaches such as ensemble phase averaging (Zhang and VanderHeyden, 2002), time averaging (Benyahia, 2008; Hrenya and Sinclair, 1997; Kallio et al., 2008) and space averaging (Igci et al., 2008; Shah et al., 2012) have been performed over the two-fluid model equations.

All these averaging approaches result for the need to develop the closure models. Kallio et al. (2008) analyzed different terms in the momentum equation to study the magnitude of the closure models by performing time averaging over the equations. In their analysis, the main terms which showed highest magnitude were the gas–solid drag force and the Reynolds stresses arising from the velocity fluctuations. Igci et al. (2008) showed in their analysis that the contribution from the Reynolds stresses is much larger than the particle phase stress and also the contribution from the drag force is much larger than the term arising from the correlation between the fluctuations in the solid volume fraction and in the pressure gradient.

During the last decade, the gas–solid drag force is the term which has received highest attention when seeking the closures for the coarse mesh simulations. For example, the approach used in the energy-minimization multi-scale (EMMS) model has concentrated only on the drag force term when performing coarse mesh simulations (Wang and Li, 2007; Yang et al., 2004). For the filtered model equations, subgrid-scale modeling of the drag force is very important. In the filtered two-fluid model equations, details about the filtered drag coefficient is presented (Igci et al., 2008). Also, in the time averaging studies by Kallio et al. (2008), the importance of correction to the drag force was presented. Coarse mesh simulation results into the loss of information about the mesoscale structures of the flow field, which leads to uniform solids concentration profiles and eventually higher solids mass flux. Thus, there is a need to correct the overestimated drag force which consequently reduces the higher solids mass flux.

Another important issue which has raised attention for the closures in the filtered two-fluid model equations is the effects caused due to the bounding walls. Igci and Sundaresan (2011) recognized the need of wall correction to the filtered drag coefficient, the filtered particle phase normal stress and the filtered particle phase shear viscosity, and formulated closure models based on the distance from the wall. Recently, Igci et al. (2012) used the idea of including the wall corrections in their simulations for different mesh sizes and obtained a reasonable agreement with experimental results. They showed that the results predicted by the filtered two-fluid model equations are nearly filter length independent. The study by Igci et al. (2012) shows the feasibility of space averaging approach in which the closure models obtained from the fine mesh simulation are applied to the coarse mesh simulation. The study of Igci and Sundaresan (2011) dealt with FCC particles belonging to Geldart group A. In the present study, a case of larger Geldart group B particles in a wider solids volume fraction range is analyzed.

In this work, the same methodology of space averaging over the two-fluid model equations as used by Igci et al. (2008) has been followed. A two-dimensional fine mesh simulation of the gas–solid flow in a CFB riser using the two-fluid model was performed in the CFD package Fluent 6.3.26. The simulation results are then space averaged over different averaging sizes to analyze the behavior of subgrid-scale models which can be used for coarse mesh simulations.

Space averaging on the two main terms, vertical component of the drag force term and the convective term, in the two-fluid model, has been performed and then the behavior of the subgrid-scale models for different averaging sizes and solid volume fraction values is analyzed. The same notations are used in this work which were defined in our prior study (Shah et al., 2012). The obtained results showed strong dependence of the subgrid-scale models on the averaging size and solid volume fraction values as a function of distance from the wall. To explain the observed behavior of the correction factor in the different averaging regions, the standard deviations of different variables were calculated to evaluate the fluctuation characteristics of the flow properties as function of the lateral coordinate.

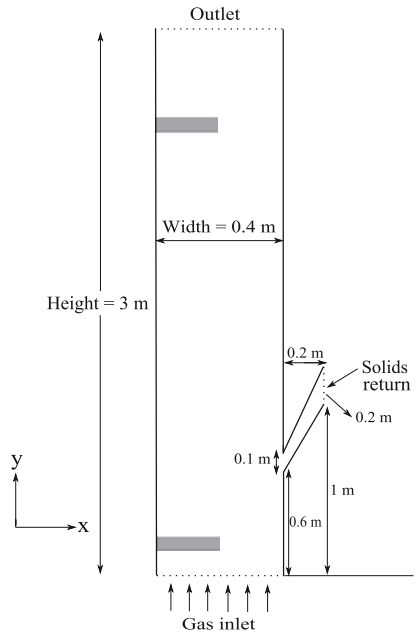

Fig. 1. Schematic drawing of the circulating fluidized bed riser and the small channel of the return leg. The selected areas seen in the lower and upper parts of the riser will be referred to later. The solid lines along the riser height and in the return leg channel represent the walls.

2. Methodology

2.1. Domain for CFD simulation

Kallio et al. (2009) give a systematic description of the experimental unit and validate the CFD modeling method by comparing measurements with results obtained from a CFD simulation, where the same models and mesh as in the present paper were used. The main components of the CFB unit include a riser, a solid separation unit, and a return leg with a loop seal. The dimensions of the CFB riser are as follows; 3 m height, 0.4 m width, and 0.015 m depth. As mentioned in Agrawal et al. (2001), ideally, 3D simulations are better than 2D simulations. In gas–solid flow systems, the qualitative analysis of heterogeneous structures can be studied by 2D simulations. In the experimental unit of our case study, we had very small depth of 0.015 m which is too small to study the fluctuations in the third direction. For this reason, our simulation was only conducted in 2D. At the bottom of the riser, an uniform gas inlet was assumed due to the difficulties in defining the computational mesh near the nozzles as located in the experiments. During the measurement, the fluidization gas velocity was 3.5 m/s and the average solids inventory in the CFB riser was about 2.5 kg. A schematic of the geometry is shown in Fig. 1.

Table 1
Governing equations and the closure models used in this study.

Gas phase (continuity and momentum equations)

$$\frac{\partial}{\partial t}(\alpha_g\rho_g)+\nabla\cdot(\alpha_g\rho_g\vec{v}_g)=0,$$
$$\frac{\partial}{\partial t}(\alpha_g\rho_g\vec{v}_g)+\nabla\cdot(\alpha_g\rho_g\vec{v}_g\vec{v}_g)=-\alpha_g\nabla p+\nabla\cdot(\bar{\bar{\tau}}_g+\alpha_g\bar{\bar{\tau}}_t)+\alpha_g\rho_g\vec{g}+K_{sg}(\vec{v}_s-\vec{v}_g).$$

Solid phase (continuity and momentum equations)

$$\frac{\partial}{\partial t}(\alpha_s\rho_s)+\nabla\cdot(\alpha_s\rho_s\vec{v}_s)=0,$$
$$\frac{\partial}{\partial t}(\alpha_s\rho_s\vec{v}_s)+\nabla\cdot(\alpha_s\rho_s\vec{v}_s\vec{v}_s)=-\alpha_s\nabla p+\nabla\cdot\bar{\bar{\tau}}_s-\nabla p_s+\alpha_s\rho_s\vec{g}+K_{gs}(\vec{v}_g-\vec{v}_s).$$

Modified $\kappa-\epsilon$ turbulence model for gas phase

$$\frac{\partial}{\partial t}(\alpha_g\rho_g\kappa)+\nabla\cdot(\alpha_g\rho_g\vec{v}_g\kappa)=\nabla\cdot\left(\alpha_g\frac{\mu_t}{\sigma_\kappa}\nabla\kappa\right)+\alpha_g\bar{\bar{\tau}}_t:\nabla\vec{v}_g-\alpha_g\rho_g\epsilon+\Pi_\kappa,$$
$$\frac{\partial}{\partial t}(\alpha_g\rho_g\epsilon)+\nabla\cdot(\alpha_g\rho_g\vec{v}_g\epsilon)=\nabla\cdot\left(\alpha_g\frac{\mu_t}{\sigma_\epsilon}\nabla\epsilon\right)+\alpha_g\frac{\epsilon}{\kappa}(C_{1\epsilon}\bar{\bar{\tau}}_t:\nabla\vec{v}_g-C_{2\epsilon}\rho_g\epsilon)+\Pi_\epsilon.$$

Granular energy equation

$$\frac{3}{2}\left[\frac{\partial}{\partial t}(\rho_s\alpha_s\Theta_s)+\nabla\cdot(\rho_s\alpha_s\vec{v}_s\Theta_s)\right]=(-p_s\bar{\bar{I}}+\bar{\bar{\tau}}_s):\nabla\vec{v}_s+\nabla\cdot(k_{\Theta_s}\nabla\Theta_s)-\gamma_{\Theta_s}+\phi_{gs}.$$

Interphase momentum exchange coefficient (Gidaspow et al., 1992)

when $\alpha_g>0.8$, $K_{gs}=\frac{3}{4}C_D\frac{\alpha_s\alpha_g\rho_g|\vec{v}_s-\vec{v}_g|}{d_s}\alpha_g^{-2.65}$,

where $C_D=\frac{24}{\alpha_g Re}[1+0.15(\alpha_g Re)^{0.687}]$ and $Re=\frac{\rho_g|\vec{v}_s-\vec{v}_g|d_s}{\mu_g}$,

when $\alpha_g\le 0.8$, $K_{gs}=150\frac{\alpha_s(1-\alpha_g)\mu_g}{\alpha_g d_s^2}+1.75\frac{\rho_g\alpha_s|\vec{v}_s-\vec{v}_g|}{d_s}$.

Phase stress–strain tensors

$$\bar{\bar{\tau}}_g=\alpha_g\mu_g(\nabla\vec{v}_g+\nabla\vec{v}_g^{\,T})-\frac{2}{3}\alpha_g\mu_g\nabla\cdot\vec{v}_g\bar{\bar{I}},\quad\text{where }\bar{\bar{I}}\text{ is the identity tensor,}$$
$$\bar{\bar{\tau}}_t=\mu_t(\nabla\vec{v}_g+\nabla\vec{v}_g^{\,T})-\frac{2}{3}(\rho_g\kappa+\mu_t\nabla\cdot\vec{v}_g)\bar{\bar{I}},\quad\text{where }\mu_t=\rho_g C_\mu\frac{\kappa^2}{\epsilon},$$
$$\bar{\bar{\tau}}_s=\alpha_s\mu_s(\nabla\vec{v}_s+\nabla\vec{v}_s^{\,T})+\alpha_s\left(\lambda_s-\frac{2}{3}\mu_s\right)\nabla\cdot\vec{v}_s\bar{\bar{I}}.$$

Turbulence exchange terms between the gas and solid phases

$$\Pi_\kappa=K_{sg}(\kappa_{sg}-2\kappa),\quad\Pi_\epsilon=C_{3\epsilon}\frac{\epsilon}{\kappa}\Pi_\kappa.$$

Covariance of the velocities of gas and solid phases

$$\kappa_{sg}=2\kappa\left(\frac{b+\eta_{sg}}{1+\eta_{sg}}\right),\quad\text{where }b=1.5\left(\frac{\rho_s}{\rho_g}+0.5\right)^{-1}\text{ and }\eta_{sg}=\frac{\tau_{t,sg}}{\tau_{F,sg}}.$$

Lagrangian integral time scale

$$\tau_{t,sg}=\frac{\frac{3}{2}C_\mu\frac{\kappa}{\epsilon}}{\sqrt{1+\frac{3}{2}(1.8-1.35\cos^2\psi)\frac{|\vec{v}_g-\vec{v}_s|^2}{\kappa}}}$$

Particle relaxation time scale

$$\tau_{F,sg}=\frac{\alpha_s\rho_g}{K_{sg}}\left(\frac{\rho_s}{\rho_g}+0.5\right).$$

Solids shear viscosity,
$\mu_s=\mu_{s,col}+\mu_{s,kin}$ (Syamlal et al., 1993) $+\mu_{s,fr}$ (Schaeffer, 1987)

$$\mu_s=\frac{4}{5}\alpha_s\rho_s d_s g_{0,ss}(1+e_{ss})\left(\frac{\Theta_s}{\pi}\right)^{1/2}+\frac{\alpha_s\rho_s d_s\sqrt{\Theta_s\pi}}{6(3-e_{ss})}\left[1+\frac{2}{5}(1+e_{ss})(3e_{ss}-1)\alpha_s g_{0,ss}\right]+\frac{p_s\sin\theta}{2\sqrt{I_{2D}}}$$

Granular bulk viscosity (Lun et al., 1984)

$$\lambda_s=\frac{4}{3}\alpha_s\rho_s d_s g_{0,ss}(1+e_{ss})\left(\frac{\Theta_s}{\pi}\right)^{1/2}.$$

Solids pressure (Lun et al., 1984)

$$p_s=\alpha_s\rho_s\Theta_s+2\rho_s(1+e_{ss})\alpha_s^2 g_{0,ss}\Theta_s.$$

Table 1 (*continued*)

Radial distribution function

$$g_{0,ss}=\left[1-\left(\frac{\alpha_s}{\alpha_{s,max}}\right)^{1/3}\right]^{-1}.$$

Diffusion coefficient for granular energy (Syamlal et al., 1993)

$$k_{\Theta_s}=\frac{15d_s\rho_s\alpha_s\sqrt{\Theta_s\pi}}{4(41-33\eta)}\left[1+\frac{12}{5}\eta^2(4\eta-3)\alpha_s g_{0,ss}+\frac{16}{15\pi}(41-33\eta)\eta\alpha_s g_{0,ss}\right],\quad\text{where}$$
$$\eta=\frac{1}{2}(1+e_{ss}).$$

Collisional dissipation of energy (Lun et al., 1984)

$$\gamma_{\Theta_s}=\frac{12(1-e_{ss}^2)g_{0,ss}}{d_s\sqrt{\pi}}\rho_s\alpha_s^2\Theta_s^{3/2}.$$

Energy exchange between the gas and solid phase

$$\phi_{gs}=-3K_{gs}\Theta_s.$$

2.2. CFD model and simulation

The two-fluid model was used for simulating the flow dynamics of the gas–solid flow in the CFB riser. There are several researchers who have performed CFD studies of the gas–solid flow in a CFB riser using the two-fluid model approach (Cabezas-Gómez et al., 2006; De Wilde et al., 2003; Hartge et al., 2009; Wang et al., 2010; Yang et al., 2004). For gas phase turbulence, a modified form of the standard $\kappa-\epsilon$ model was used with extra terms that include the interphase turbulence exchange terms. The closure models for the solid phase momentum equation are based on the kinetic theory of granular flow. In addition to the continuity and momentum equations for both phases, the granular energy equation is solved for calculating the granular temperature, which is then used to close the terms solid phase stress and solids pressure. The governing equations and the selected closure models used in this study are listed in Table 1.

The phase coupled SIMPLE algorithm was used for pressure-velocity coupling. The first order implicit for time-stepping, the first order upwind for volume fraction, and the second order upwind for the other convective terms were used as discretization schemes. The relative error between two successive iterations for each scaled residual component was below 1e−03 for most of the time steps. For the boundary conditions at the walls, the free-slip condition was used for the gas phase and Johnson and Jackson's model of the partial-slip condition with a value of 0.001 for the specularity coefficient and a value of 0.2 for the particle-wall restitution coefficient was used for the solid phase. Same values were used in Kallio et al. (2009) where a good fit to measurement data was obtained. The mass flow rate of solids at the solids return was kept the same as that at the outlet, thus maintaining the overall solid volume fraction in the riser as constant. The total simulation time was 215 s, in which the first 35 s was used to obtain the stable state operating condition, and the averaging and post-processing of the results were performed over the last 180 s. A summary of the parameters used in the CFD simulation are listed in Table 2. Although the fine mesh and short time step considered here are not highly resolved to study the smallest fluctuations in the flow field, they still capture essential features when performing the simulation. The same time step and mesh spacing were used in Kallio et al. (2011) where the simulated and measured variances of solid volume fraction showed good agreement.

3. Results and discussion

3.1. Space averaging on the drag model

In this work, a fine mesh simulation of the gas–solid flow in a CFB riser using the two-fluid model was performed. The mesh cell size used in the simulation was $0.625 \times 0.625\ \text{cm}^2$ (The aspect ratio $\delta x : \delta y$ in this simulation was 1:1). Space averaging was applied on the drag model for three different averaging sizes, $1.25 \times 1.25\ \text{cm}^2$, $2.5 \times 2.5\ \text{cm}^2$, and $5 \times 5\ \text{cm}^2$. Shah et al. (2012) studied the effect of different time step sizes in simulations and the difference was insignificant at least in the range investigated. Thus, no time averaging is considered here. The same type of notations are used here which were used in our previous study (Shah et al., 2012). For a constant time scale, the space averaging on the vertical drag force model can be mathematically given as

$$^{\Delta x}\langle {}^{\delta x}_{\delta t}(K_{gs}(v_{g,y}-v_{s,y}))\rangle = \omega K^{*}_{gs}(\tilde{v}_{g,y}-\tilde{v}_{s,y}), \tag{1}$$

where ω is the correction factor for the drag force term to be found, K^{*}_{gs} is the interphase momentum exchange coefficient calculated from averaged variables, and $\tilde{v}_{g,y}$ and $\tilde{v}_{s,y}$ are the averaged phase velocities defined accordingly as

$$\tilde{v}_{g,y} = \frac{^{\Delta x}\langle {}^{\delta x}_{\delta t}(\alpha_g v_{g,y})\rangle}{^{\Delta x}\langle {}^{\delta x}_{\delta t}\alpha_g\rangle} \quad \text{and} \quad \tilde{v}_{s,y} = \frac{^{\Delta x}\langle {}^{\delta x}_{\delta t}(\alpha_s v_{s,y})\rangle}{^{\Delta x}\langle {}^{\delta x}_{\delta t}\alpha_s\rangle}. \tag{2}$$

In this study, the mesh spacing in the transient simulation, δx, is 0.625 cm and the time step, δt, is 0.001 s. The region over which the averaging is carried out is given as Δx. On the left-hand side of Eq. (1), the transient values of the vertical drag force were calculated for the cells with size $0.625 \times 0.625\ \text{cm}^2$ for the selected areas in the lower and upper parts of the riser (see Fig. 1). These transient values of the vertical drag force are averaged over the cells which fit to the different averaging sizes (for example, 4 cells with the averaging size $1.25 \times 1.25\ \text{cm}^2$, 16 cells with the averaging size $2.5 \times 2.5\ \text{cm}^2$, and 64 cells with the averaging size $5 \times 5\ \text{cm}^2$). Thus, a transient series of the averaged vertical drag force is obtained as the left-hand side of Eq. (1). On the right-hand side of Eq. (1), the same logic has been applied for the drag force model which is calculated based on the averaged variables defined according to Eq. (2).

The correction factor ω can be written as the ratio of the averaged drag force and the drag force calculated from averaged

Table 2
Summary of parameters for the CFD simulation.

Gas density, ρ_g	1.225 kg/m^3
Gas viscosity, μ_g	1.7894×10^{-5} kg/ms
Solid particle density, ρ_s	2480 kg/m^3
Solid particle diameter, d_s	385×10^{-6} m
Fluidization gas velocity	3.5 m/s
Mesh cell size (cm^2)	0.625×0.625
Time step size (s)	0.001
Maximum packing limit, $\alpha_{s,max}$	0.63
Restitution coefficient, e_{ss}	0.9

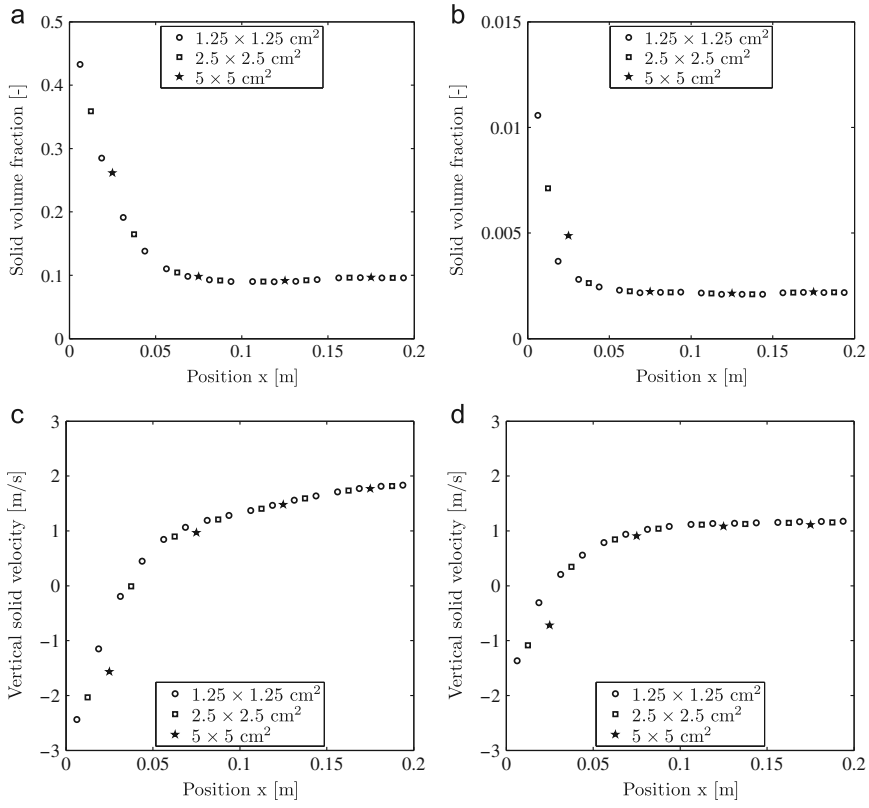

Fig. 2. Profiles of time-averaged values of solid volume fraction and vertical solid velocity for different averaging sizes. (a and c) The profiles at the height $y=0.175$ m and (b and d) the profiles at the height $y=2.475$ m.

variables. Time instant values of correction factors can be obtained for the different regions of the averaging sizes $1.25 \times 1.25\ cm^2$, $2.5 \times 2.5\ cm^2$, and $5 \times 5\ cm^2$. The statistical averages of correction factor values based on the approximate bin size of 0.008 of averaged solid volume fraction were calculated.

3.1.1. Averaged profiles in horizontal direction

To be able to interpret the results on the correction factor, it is useful to first study the horizontal profiles of the solid volume fraction and the vertical solid velocity. This is done in this section at two different heights for different averaging sizes. Fig. 2a and b shows the averaged (in time) profiles of the solid volume fraction for different averaging sizes. The profiles show similar behavior for different averaging sizes with high concentration near the walls and lower concentration towards the center of the riser. Fig. 2c and d shows the averaged (in time) profile of the vertical solid velocity for different averaging sizes calculated according to Eq. (2). From the velocity profiles, the downflow region of solids at the wall for different averaging sizes can be observed. For the averaging size of $1.25 \times 1.25\ cm^2$, the profile shows that solids flow downward within the distance of 0.0375 m in the lower part and 0.025 m in the upper part from the wall of the riser. As the size of the averaging region increases, the detailed information on the velocity and volume fraction trends in the wall region is lost. Similar loss of information on the averaged profiles is not observed in the riser center.

3.1.2. Fluctuation characteristics using standard deviation

In Igci and Sundaresan (2011) and Shah et al. (2012), the drag correction factor monotonously reduced towards the walls. Igci and Sundaresan (2011) gave as an explanation to this trend that clustering increases towards to the walls. The variation in the solid volume fraction can be used as an indicator of the level of clustering, i.e. how strongly the volume fraction is divided into dense and dilute values. In the literature, the characteristics of solid volume fraction fluctuation have been studied in experimental as well as computational analysis of gas–solid flows in CFB risers. Issangya et al. (2000) studied the standard deviation of the voidage for different solids flux and superficial air velocity conditions in a high-density CFB riser. Wang (2008) performed high-resolution Eulerian simulation and studied the solid volume fraction fluctuation using the root mean square approach. Kallio et al. (2011) presented the fluctuation characteristics of the solid volume fraction in a CFB and observed similar trends in results obtained from experimental measurements and CFD simulations. The fluctuations are, by definition, zero at zero volume fraction and at the packing limit. Fluctuations in the solid volume fraction are presented by a roughly parabolic curve as a function of the average solid volume fraction, with the peak at half of the volume fraction of a packed bed, i.e. around solid volume fraction of about 0.3. In Kallio et al. (2011) it was observed in a similar study of Geldart group B particles that at the same average volume fraction in the wall layer and in the core, the volume fraction fluctuations are stronger in the core than at the wall, which is contrary to what was stated by Igci and Sundaresan (2011).

To further study the validity of the explanation by Igci and Sundaresan (2011), the variations in the solid volume fraction and other flow properties are studied in the following. Several variables and combinations of variables were investigated of which the most interesting ones are shown here. Fig. 3 shows the variation in the standard deviations of solid volume fraction, slip velocity and drag coefficient for different averaging sizes. The analysis is here presented at the height of $y = 0.175$ m where the solid volume fraction varies in a wide range. Fig. 3 clearly shows

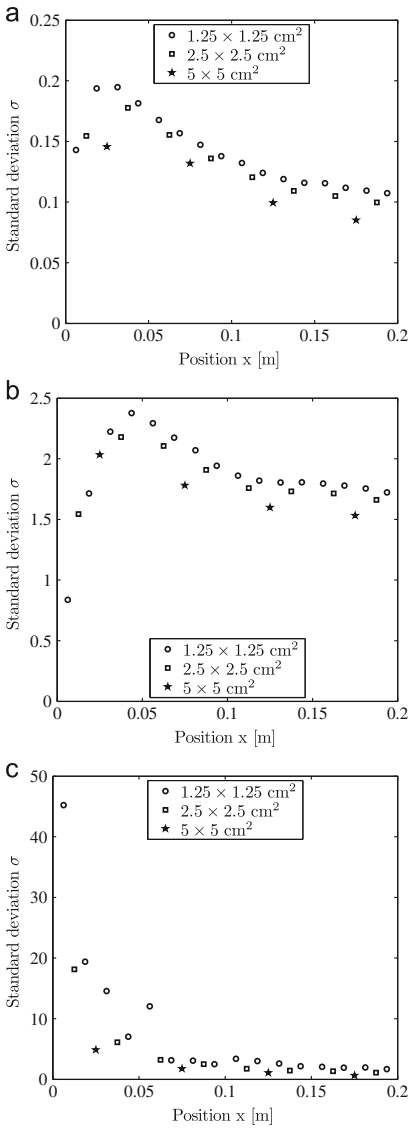

Fig. 3. Standard deviation of (a) solid volume fraction, (b) slip velocity and (c) drag coefficient for different averaging sizes. The analysis was carried out at the height $y = 0.175$ m.

the dependence of standard deviation values with the averaging sizes. The standard deviation values start to decrease as the averaging size is increased. In Fig. 3a, the peak in the standard deviation profile indicates that there is the largest solid volume fraction fluctuation a couple of centimeters from the wall, where the average solid volume fraction is close to 0.3, which is in accordance with the observations in the literature. The behavior of the standard deviation of slip velocity is quite similar to the standard deviation of solid volume fraction.

It can be seen from Fig. 3 that the fluctuations of solid volume fraction and slip velocity do not give any explanation for the lower values of the correction factor near the walls. According to our analysis, the term in the drag model which gives higher

fluctuations near the walls was C_D. The mathematical model of C_D itself contains the correlation of voidage and slip velocity, which might be interpreted as the reason for higher fluctuations near the wall.

To further evaluate the reason for the low drag correction factor at the wall, the fluctuations in the slip velocity and the drag coefficient were studied for different values of solid volume fractions. Fig. 4a–c shows the standard deviation of the slip velocity for different averaging sizes. It can be seen from the figure that the variation in the slip velocity does not clearly differentiate the wall region and the center region. Fig. 5a–c shows the standard deviation of the single particle drag coefficient for different averaging sizes. Magnitude of the fluctuation of the single particle drag coefficient increases with the values of the

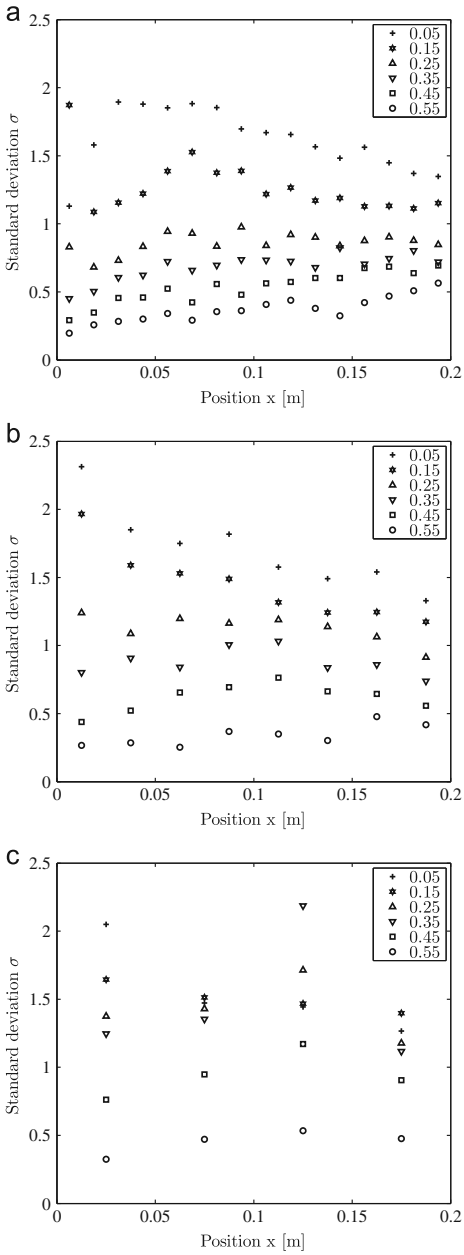

Fig. 4. Standard deviation of slip velocity for different values of solid volume fractions inside the averaging region for averaging sizes (a) 1.25×1.25 cm^2, (b) 2.5×2.5 cm^2 and (c) 5×5 cm^2. The analysis was carried out at the height y=0.175 m.

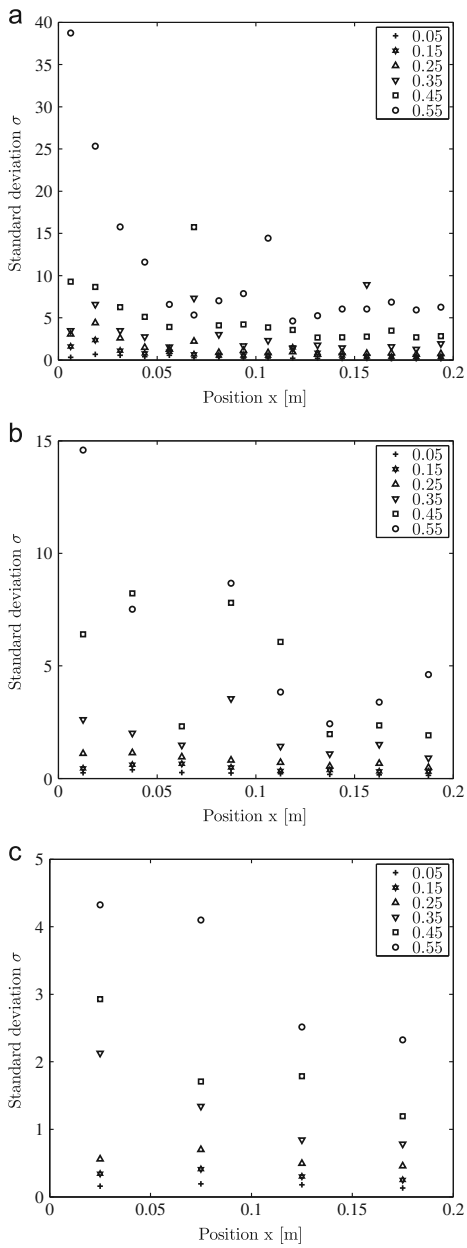

Fig. 5. Standard deviation of single particle drag coefficient for different values of solid volume fractions inside the averaging region for averaging sizes (a) 1.25×1.25 cm^2, (b) 2.5×2.5 cm^2 and (c) 5×5 cm^2. The analysis was carried out at the height y=0.175 m.

solid volume fraction. However, no uniform trend as function of the distance to the wall can be detected. For low solid volume fractions the variations in slip velocity have a tendency to increase towards the walls whereas for high solid volume fractions the fluctuations in the drag coefficient increase towards the walls. The decrease of the drag correction factor towards the walls is thus likely to be a result of complicated interactions between the primary variables and not a direct result of stronger clustering at the wall as was suggested by Igci and Sundaresan (2011).

3.1.3. Effect of solid volume fraction

In this section, we study the variation of the correction factor for different values of solid volume fractions in the averaging region as a function of the distance from the wall. The corresponding behavior of the correction factor for different values of solid volume fraction is shown in Fig. 6 for three different averaging sizes. In their analysis, Igci and Sundaresan (2011) noted that the minimum number of samples over which their statistical averages were carried out was 1000. In our analysis, for lower and moderate values of solid volume fractions, the number of samples was well above 1000. However, for higher values of solid volume fractions, the number of samples was below 1000. We want to note that the somewhat stochastic results shown in the figure for higher values of solid volume fractions may be related to not having a big enough number of samples during averaging. The general trends are still clear. At most solid volume fractions, the smallest values for the correction factor are observed in the wall layer, with a minimum at the location closest to the wall. Fig. 6a–c clearly shows the dependence of correction factor values with respect to solid volume fractions. The correction factor starts to decrease as the averaging size is increased and this observation is similar to the findings of previous works (De Wilde, 2005; Igci et al., 2008). For all the three averaging size cases, the minimum values of the correction factor lies in between the solid volume fraction values of 0.25–0.35 indicating that in this solids concentration range, a big correction to the drag force is necessary. This is understandable since this range of average solid volume fraction allows the largest local variation in the volume fractions produced by the original fine mesh simulation. The low and high average solid concentrations indicate a more uniform suspension density. In the next section, we study the more detailed behavior of the correction factor for different solid volume fraction values.

3.1.4. Effect of averaging sizes

The behavior of the correction factor for the three averaging sizes is shown in Fig. 7 for different values of solid volume fractions. The analysis was done for the selected area in the lower part of the riser so that the whole solid volume fraction range can be considered. Fig. 7a–e shows that in this moderate solid volume fraction range, there is a clear dependence of the correction factor with the averaging sizes. The correction factor decreases as the averaging size is increased. However, this type of behavior is not clearly seen for the higher solid volume fraction range and the curves represent more stochastic behavior as in Fig. 7f–h. Near the packing limit, Fig. 7i shows that the correction factor starts to tend towards unity for all the averaging sizes.

The behavior of the correction factor for three averaging sizes is shown in Fig. 8 for the selected area in the upper part of the riser. Since the suspension is dilute in the upper part of the riser, only one value of solid volume fraction, $\alpha_s = 0.005$ was considered. In the upper part of the riser also the correction factor profiles are dependent on the averaging size. In Igci and Sundaresan (2011) it was observed that the filtered drag coefficient could be normalized such that the correction as a function of the distance to the wall would become independent of averaging size and average solid volume fraction. Fig. 7 shows that the correction factors obtained in this work for Geldart group B particles in a wider solid volume fraction range cannot be expressed as a single function by normalizing the values.

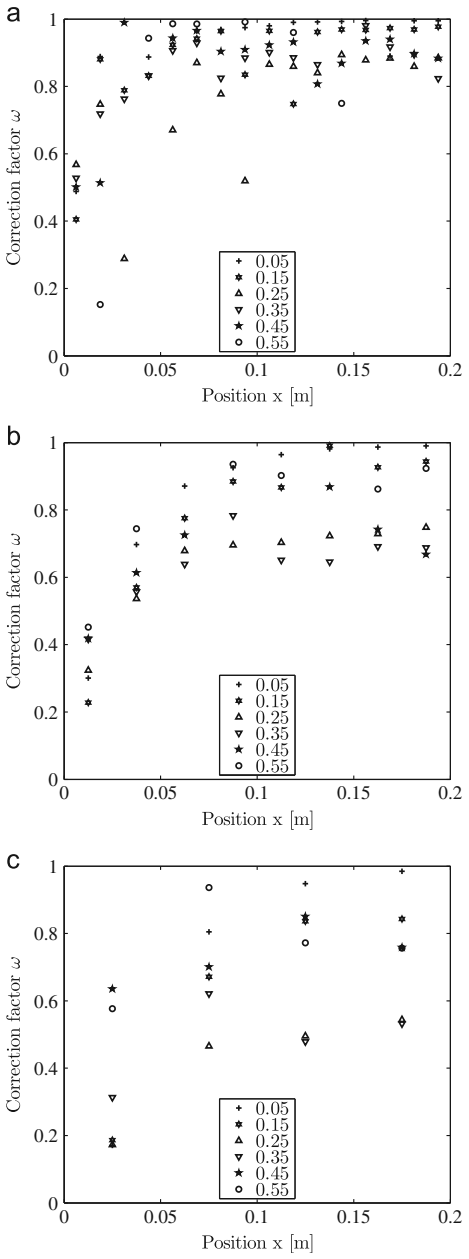

Fig. 6. Correction factor with respect to distance from the wall with different solid volume fractions inside the averaging region for averaging sizes (a) 1.25×1.25 cm^2, (b) 2.5×2.5 cm^2 and (c) 5×5 cm^2. The analysis was carried out at the height $y = 0.175$ m.

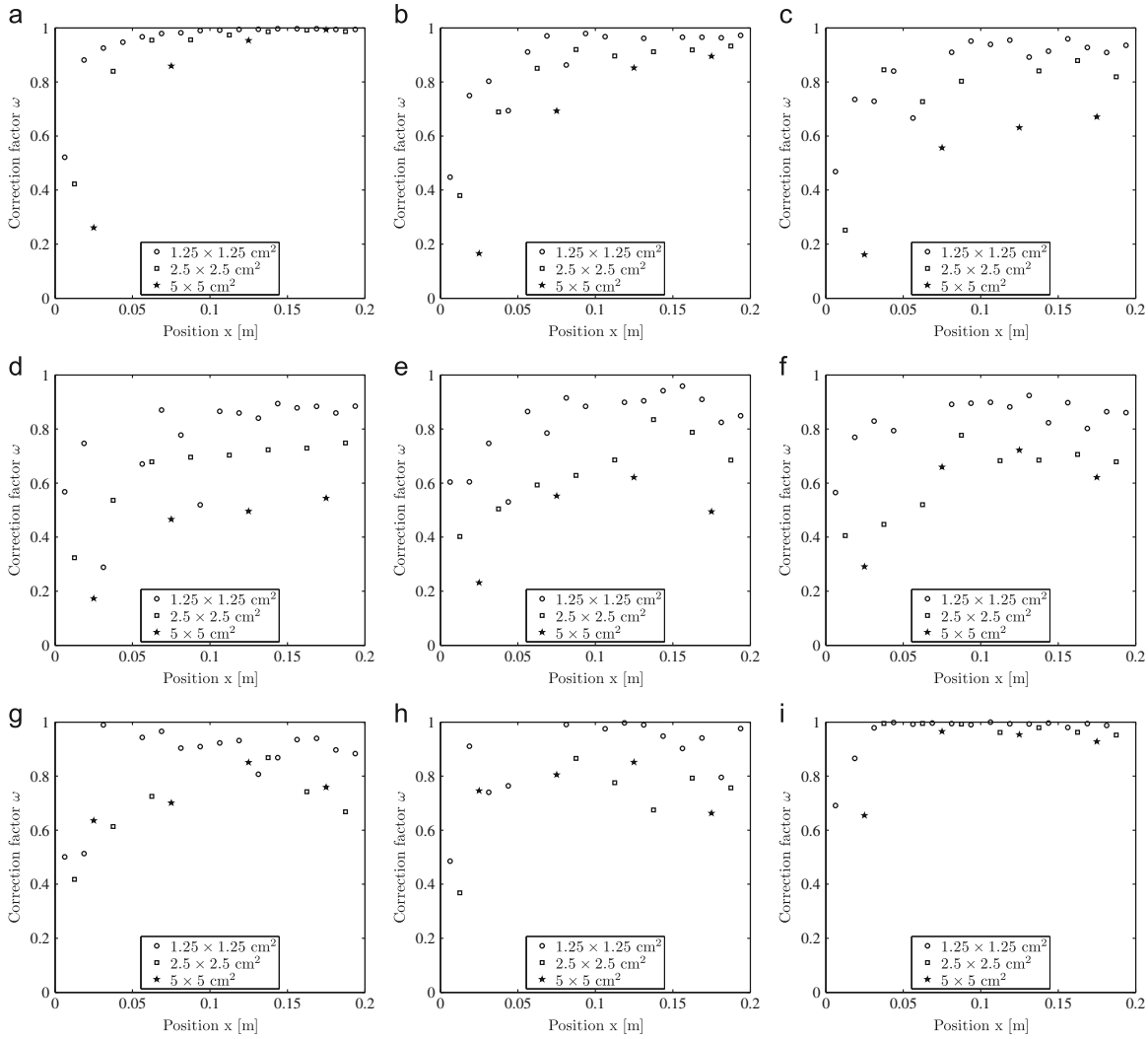

Fig. 7. Correction factor with respect to distance from the wall with different averaging sizes for solid volume fractions inside the averaging region as (a) 0.01, (b) 0.125, (c) 0.2, (d) 0.25, (e) 0.3, (f) 0.375, (g) 0.45, (h) 0.525, and (i) 0.6. The analysis was carried out at the height $y=0.175$ m.

3.2. Space averaging on the convective term

Another important term which is being analyzed in the study is the convective term. The convective term of the solid phase momentum equation is space averaged to obtain the contribution of the Reynolds stresses due to the fluctuations in the solid phase velocities. For example, in the mathematical notations, the normal Reynolds stress components can be written as,

$$^{\Delta x}\langle \tfrac{\delta x}{\delta t}(\alpha_s \rho_s v_{s,x} v_{s,x})\rangle = \overline{\alpha}_s \rho_s \tilde{v}_{s,x}\tilde{v}_{s,x} + \text{Reynolds stress}, \quad (3)$$

$$^{\Delta x}\langle \tfrac{\delta x}{\delta t}(\alpha_s \rho_s v_{s,y} v_{s,y})\rangle = \overline{\alpha}_s \rho_s \tilde{v}_{s,y}\tilde{v}_{s,y} + \text{Reynolds stress}, \quad (4)$$

where $\overline{\alpha}_s$ is the averaged solid volume fraction inside the averaging region.

The behavior of the horizontal and vertical normal Reynolds stress components for different averaging sizes is shown in Figs. 9 and 10. It is clearly seen from both figures that the behavior of the Reynolds stress components is very much dependent on the averaging size and the magnitude increases as the averaging size is increased. Similar to the correction factor for the drag force, the normal Reynolds stress component shows higher values near the walls. It is seen from the figures that the magnitude of the vertical normal Reynolds stress component is much larger than the horizontal component. The wall effects must be considered in modeling of the Reynolds stresses in such filtered model equations.

4. Conclusions

Fine mesh CFD simulations of gas–solid two-phase flow in a CFB riser with a two-fluid model are very time consuming and hence require a coarse mesh and consequently filtered model

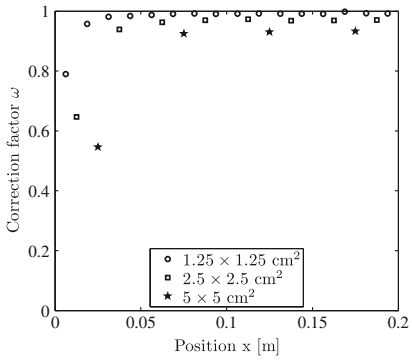

Fig. 8. Correction factor with respect to distance from the wall with different averaging sizes for the value of solid volume fraction as $\alpha_s = 0.005$. The analysis was carried out at the height $y = 2.475$ m.

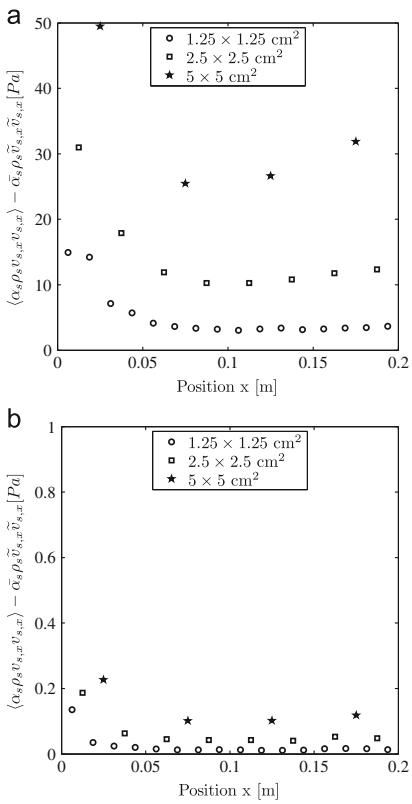

Fig. 9. Horizontal normal Reynolds stress component for different averaging sizes at two different heights: (a) $y = 0.175$ m and (b) $y = 2.475$ m.

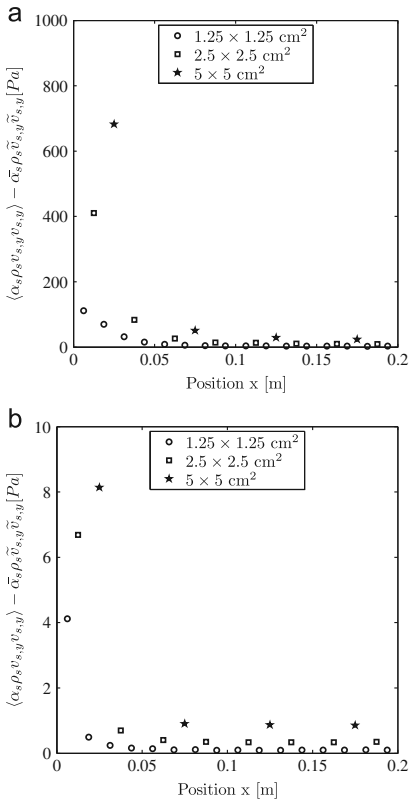

Fig. 10. Vertical normal Reynolds stress component for different averaging sizes at two different heights: (a) $y = 0.175$ m and (b) $y = 2.475$ m.

equations. The main challenge with the filtered two-fluid model equations is the closure of the terms which result after macroscopic averaging over the equations. In this paper, a two-dimensional fine mesh simulation of the gas–solid flow in a CFB riser was performed for a case of Geldart group B particles. Space averaging on the vertical component of the drag force and the convective term was carried out in the lower and upper areas of the riser for different averaging sizes. The goal was to study the behavior of the subgrid-scale models for different averaging sizes and a wide range of solid volume fractions.

Subgrid-scale models to be applied for both the drag force and the normal components of solid phase Reynolds stress, were strongly dependent on the averaging size. Larger averaging sizes show higher magnitude in the values of the subgrid-scale models. Although the fluctuations in the solid volume fraction, related to the amount of clustering, did not always increase up to the wall, the maximum magnitude of the correction for the drag force was in all cases found at locations closest to the wall. One explanation for this observation was found in the strong fluctuation in the value of the drag coefficient in the downflow region at the wall. A clear dependence of the correction factor values of the drag force model on the distance to the wall was obtained for the lower and moderate range of solid volume fractions. At higher values of the solid volume fractions, the behavior of the correction factor was somewhat stochastic for all the averaging sizes considered here, but this could have been a result of not having a sufficient amount of data for averaging out the fluctuations in all cases. At the maximum packing limit and in very dilute conditions, the drag correction factor values were tending towards unity. In the solid phase momentum equation, the normal components of the Reynolds stress also show higher magnitude towards the walls. Thus, there is a need to formulate proper expressions for the subgrid-scale models which take into account the effects of averaging size, solid volume fraction and distance from the wall. The formulation and validation of this kind of correlations is a scope of future research activities.

Nomenclature

Symbols

$\overline{\overline{I}}$	identity tensor
$\overrightarrow{g}$	acceleration due to gravity (m/s^2)
$\overrightarrow{v}_i$	phase velocity (m/s)
$\check{v}_i$	averaged phase velocity (m/s)
C_D	drag coefficient for a particle
$C_\mu, C_{1\epsilon}, C_{2\epsilon}, C_{3\epsilon}$	constants in the gas turbulence model with values 0.09, 1.44, 1.92, and 1.2, respectively
d_i	particle diameter (m)
e_i	restitution coefficient
$g_{0,i}$	radial distribution function
I_{2D}	second invariant of the deviatoric stress tensor
K_i^*	interphase momentum exchange coefficient calculated from averaged variables, kg/m^3 s
K_i	interphase momentum exchange coefficient (kg/m^3 s)
k_{Θ_s}	diffusion coefficient for granular energy (kg/ms)
p	pressure (kg/ms^2)
Re	relative Reynolds number

Greek alphabets

α	volume fraction
$\overline{\alpha}$	averaged volume fraction
$\overline{\overline{\tau_i}}$	stress–strain tensor (kg/ms^2)
δt	time step size (s)
δx	mesh size in horizontal direction (m)
δy	mesh size in vertical direction (m)
ϵ	turbulent dissipation rate (m^2/s^3)
γ_{Θ_s}	collisional dissipation of energy (kg/m s^3)
κ	turbulent kinetic energy (m^2/s^2)
$\tau_{t,sg}$	Lagrangian integral time scale
$\tau_{F,sg}$	particle relaxation time scale
Π	turbulence exchange terms between gas and solid phases
σ	standard deviation
$\sigma_\kappa, \sigma_\epsilon$	constants in the gas turbulence model with values 1.0 and 1.3, respectively
λ_i	bulk viscosity (kg/ms)
μ_i	shear viscosity (kg/ms)
ω	correction factor
ϕ_i	energy exchange between the gas and solid phase (kg/ms^3)
ρ	density (kg/m^3)
θ	angle of internal friction
ψ	angle between mean particle velocity and mean relative velocity
Θ_i	granular temperature (m^2/s^2)

Subscripts

g	gas
i	general index
s	solid
t	turbulent

Acknowledgments

The authors from LUT Energy would like to acknowledge the financial support for this research from the Academy of Finland under Grant 124368. Srujal Shah is also grateful for the financial support for this research from the Academy of Finland under the project 'The Finnish Graduate School in Computational Fluid Dynamics'.

References

Agrawal, K., Loezos, P., Syamlal, M., Sundaresan, S., 2001. The role of meso-scale structures in rapid gas–solid flows. J. Fluid Mech. 445, 151–185.
Anderson, T.B., Jackson, R., 1967. A fluid mechanical description of fluidized beds. Ind. Eng. Chem. Fundam. 6, 527–539.
Benyahia, S., 2008. A time-averaged model for gas–solids flow in a one-dimensional vertical channel. Chem. Eng. Sci. 63, 2536–2547.
Benyahia, S., Syamlal, M., O'Brien, T., 2007. Study of the ability of multiphase continuum models to predict core-annulus flow. AIChE J. 53, 2549–2568.
Cabezas-Gómez, L., Silva, R.C., Milioli, F.E., 2006. Some modeling and numerical aspects of the two-fluid simulation of the gas–solids flow in a CFB riser. Braz. J. Chem. Eng. 23, 487–496.
De Wilde, J., 2005. Reformulating and quantifying the generalized added mass in filtered gas–solid flow models. Phys. Fluids 17, 113304.
De Wilde, J., Marin, G.B., Heynderickx, G.J., 2003. The effects of abrupt T-outlets in a riser: 3D simulation using the kinetic theory of granular flow. Chem. Eng. Sci. 58, 877–885.
Gidaspow, D., 1994. Multiphase Flow and Fluidization: Continuum and Kinetic Theory Descriptions. Academic Press, San Diego.
Gidaspow, D., Bezburuah, R., Ding, J., 1992. Hydrodynamics of circulating fluidized beds: kinetic theory approach. In: Potter, O., Nicklin, D. (Eds.), Proceedings of the 7th Engineering Foundation Conference on Fluidization. Brisbane, pp. 75–82.
Hartge, E.U., Ratschow, L., Wischnewski, R., Werther, J., 2009. CFD-simulation of a circulating fluidized bed riser. Particuology 7, 283–296.
Hrenya, C., Sinclair, J., 1997. Effects of particle-phase turbulence in gas–solid flows. AIChE J. 43, 853–869.
Igci, Y., Andrews, A.T., Sundaresan, S., Pannala, S., O'Brien, T., 2008. Filtered two-fluid models for fluidized gas–particle suspensions. AIChE J. 54, 1431–1448.
Igci, Y., Pannala, S., Benyahia, S., Sundaresan, S., 2012. Validation studies on filtered model equations for gas–particle flows in risers. Ind. Eng. Chem. Res. 51, 2094–2103.
Igci, Y., Sundaresan, S., 2011. Verification of filtered two-fluid models for gas–particle flows in risers. AIChE J. 57, 2691–2707.
Issangya, A.S., Grace, J.R., Bai, D., Zhu, J., 2000. Further measurements of flow dynamics in a high-density circulating fluidized bed riser. Powder Technol. 111, 104–113.
Kallio, S., Guldén, M., Hermanson, A., 2009. Experimental study and CFD simulation of a 2D circulating fluidized bed. In: Yue, G., Zhang, H., Zhao, C., Luo, Z. (Eds.), Proceedings of the 20th International Conference on Fluidized Bed Combustion. Xi'an, pp. 799–804.
Kallio, S., Peltola, J., Taivassalo, V., 2011. Characteristics of the solid volume fraction fluctuations in a CFB. In: Knowlton, T. (Ed.), Proceedings of the 10th International Conference on Circulating Fluidized Beds and Fluidization Technology. Sunriver, pp. 561–568.
Kallio, S., Taivassalo, V., Hyppänen, T., 2008. Towards time-averaged CFD modelling of circulating fluidized beds. In: Werther, J., Nowak, W., Wirth, K.E., Hartge, E.U. (Eds.), Circulating Fluidized Bed Technology IX. Hamburg, pp. 259–264.
Lun, C.K.K., Savage, S.B., Jeffrey, D.J., Chepurniy, N., 1984. Kinetic theories for granular flow: inelastic particles in Couette flow and slightly inelastic particles in a general flowfield. J. Fluid Mech. 140, 223–256.
Schaeffer, D., 1987. Instability in the evolution equations describing incompressible granular flow. J. Differ. Equations 66, 19–50.
Shah, S., Ritvanen, J., Hyppänen, T., Kallio, S., 2012. Space averaging on a gas–solid drag model for numerical simulations of a CFB riser. Powder Technol. 218, 131–139.
Syamlal, M., Rogers, W., O'Brien, T., 1993. MFIX Documentation: Theory Guide. Technical Report. DOE/METC-94/1004, DE94000087, Morgantown, WV.
Wang, J., 2008. High-resolution Eulerian simulation of RMS of solid volume fraction fluctuation and particle clustering characteristics in a CFB riser. Chem. Eng. Sci. 63, 3341–3347.
Wang, W., Li, J., 2007. Simulation of gas–solid two-phase flow by a multi-scale CFD approach—extension of the EMMS model to the sub-grid level. Chem. Eng. Sci. 62, 208–231.
Wang, X., Jin, B., Zhong, W., Xiao, R., 2010. Modeling on the hydrodynamics of a high-flux circulating fluidized bed with Geldart group A particles by kinetic theory of granular flow. Energy Fuels 24, 1242–1259.
Yang, N., Wang, W., Ge, W., Wang, L., Li, J., 2004. Simulation of heterogeneous structure in a circulating fluidized-bed riser by combining the two-fluid model with the EMMS approach. Ind. Eng. Chem. Res. 43, 5548–5561.
Zhang, D., VanderHeyden, W., 2002. The effects of mesoscale structures on the macroscopic momentum equations for two-phase flows. Int. J. Multiphase Flow 28, 805–822.